Supplementary information

Temperature-adaptive metasurface radiative cooling device with excellent emittance and low solar absorptance for dynamic thermal regulation

Junlin Yang, Qianyi Li, Shiqiao Liu, Debao Fang, Jingyao Zhang, Haibo Jin *, Jingbo Li *

Beijing Key Laboratory of Construction Tailorable Advanced Functional Materials and Green Applications, School of Materials Science and Engineering, Beijing Institute of Technology, Beijing 100081, China

* Corresponding author.

E-mail address: lijb@bit.edu.cn; hbjin@bit.edu.cn

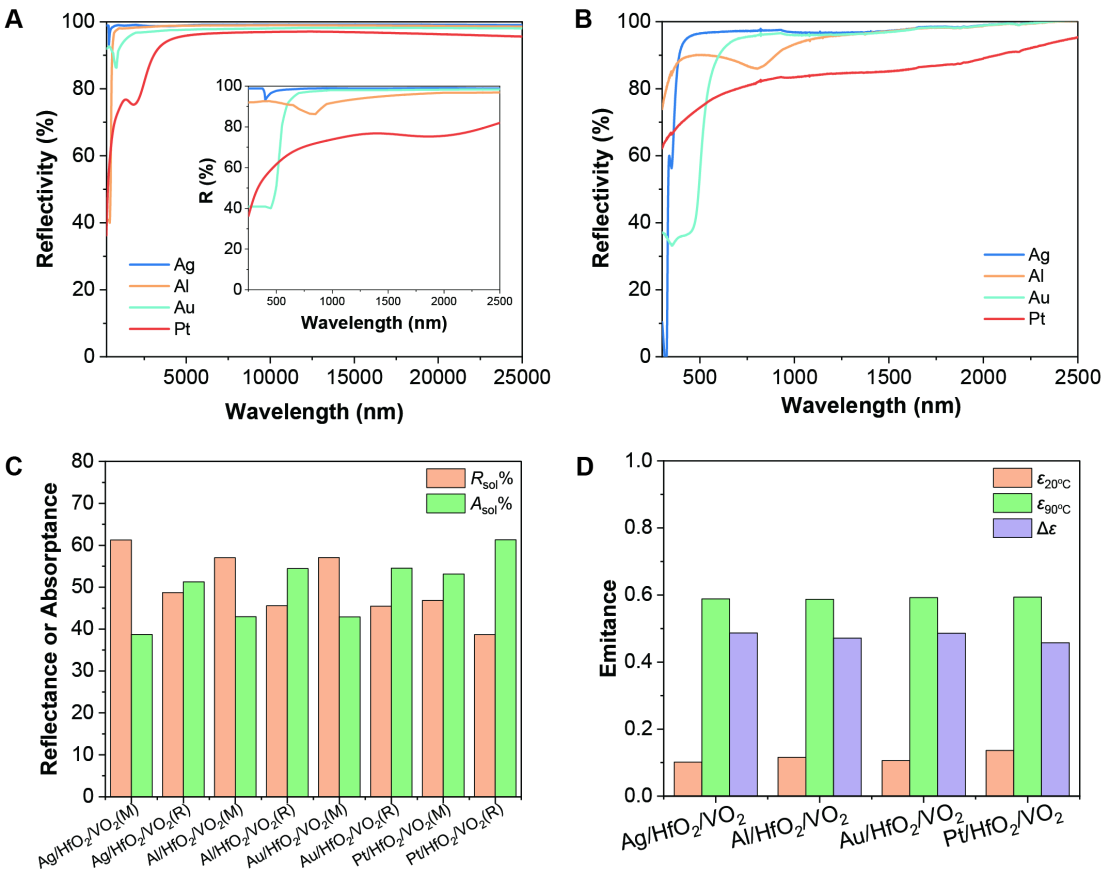

Fig. S1 (A) Simulated reflectivity of different metals. (B) Measured reflectivity of different metals. (C) Simulated solar reflectance and absorptance of radiative cooling devices with different metal substrates. (D) The stimulated emittance of radiative cooling devices with varying substrates of metal.

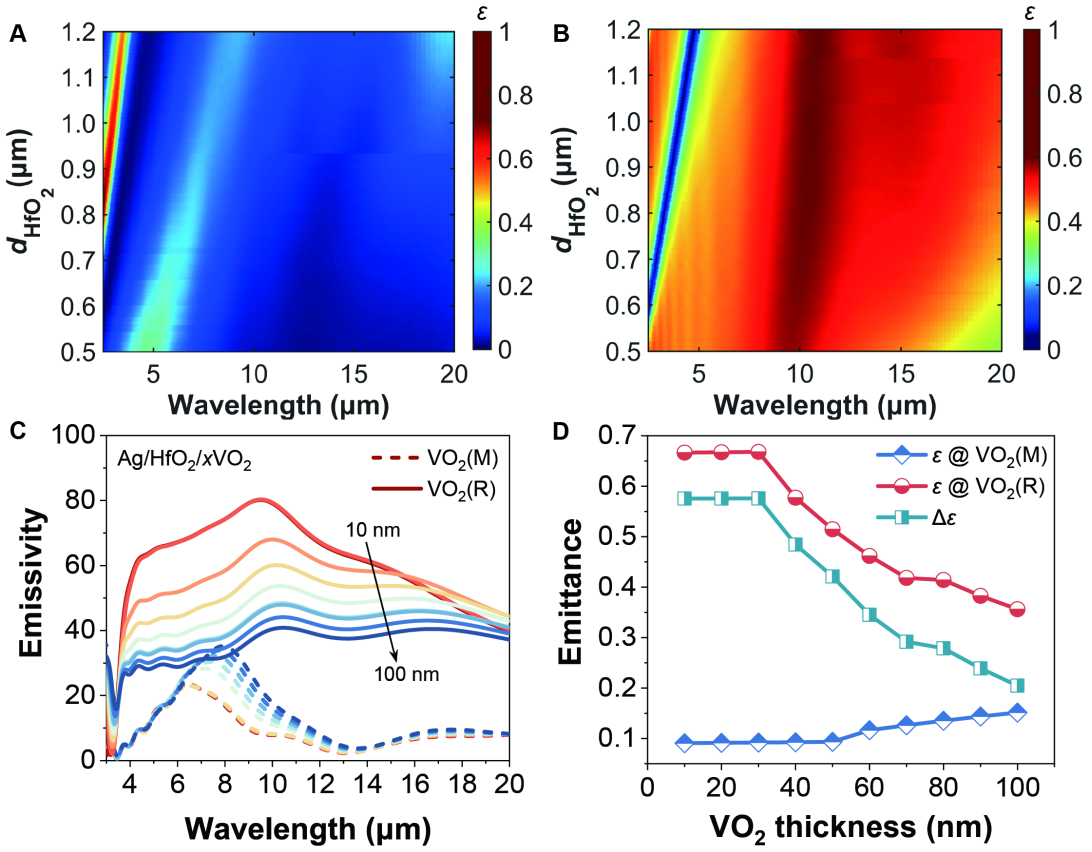

Fig. S2 Calculated emissivity mapping as a function of the HfO_2 thickness for the ATRD in the insulator (A) and metal (B) states. (C) Simulated emissivity spectra as a function of the VO_2 thickness for the ATRD in insulator (dotted line) and metallic (solid line) states. (D) The calculated emittance and emittance tunability ($\Delta\varepsilon$) as a function of VO_2 thickness.

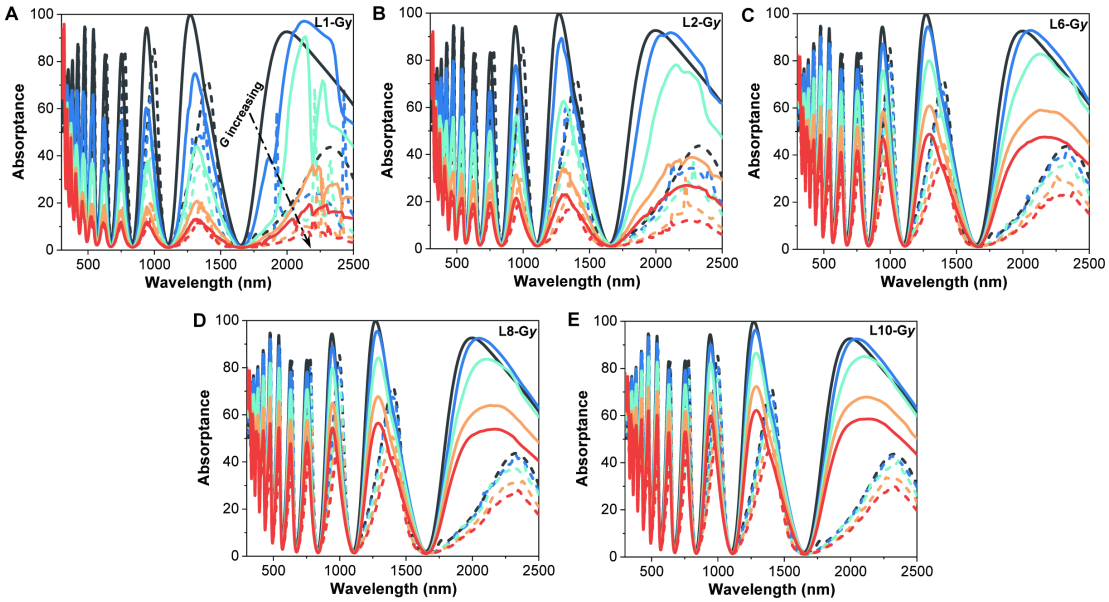

Fig. S3 The simulated solar absorptance spectra for ATMRD L*x*-G*y* samples with x = 1, 2, 6, 8 and 10 μm and y = 0.5, 1, 2 and 3 μm. Here, the dotted and solid lines represent the insulator and metal states of VO_2, respectively. The dark line represents the solar absorptance spectra of ATRD.

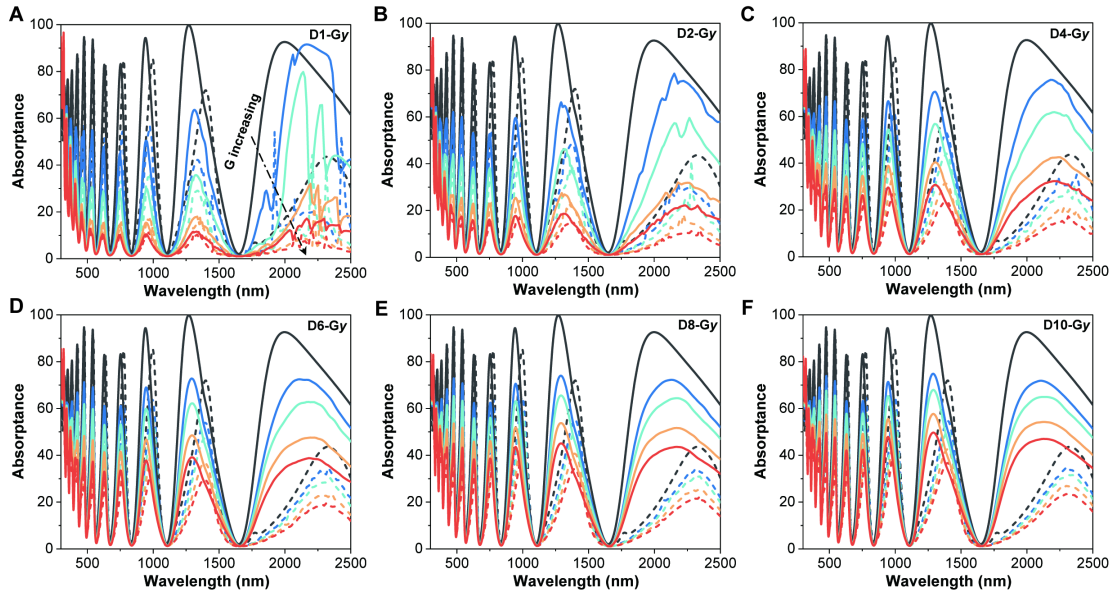

Fig. S4 The simulated solar absorptance spectra for ATMRD with circular array structure. Here, the dotted and solid lines represent the insulator and metallic states of VO_2, respectively. The dark gray line represents the solar absorptance spectra of ATRD. Here, the dotted and solid lines represent the insulator and metal states of VO_2, respectively.

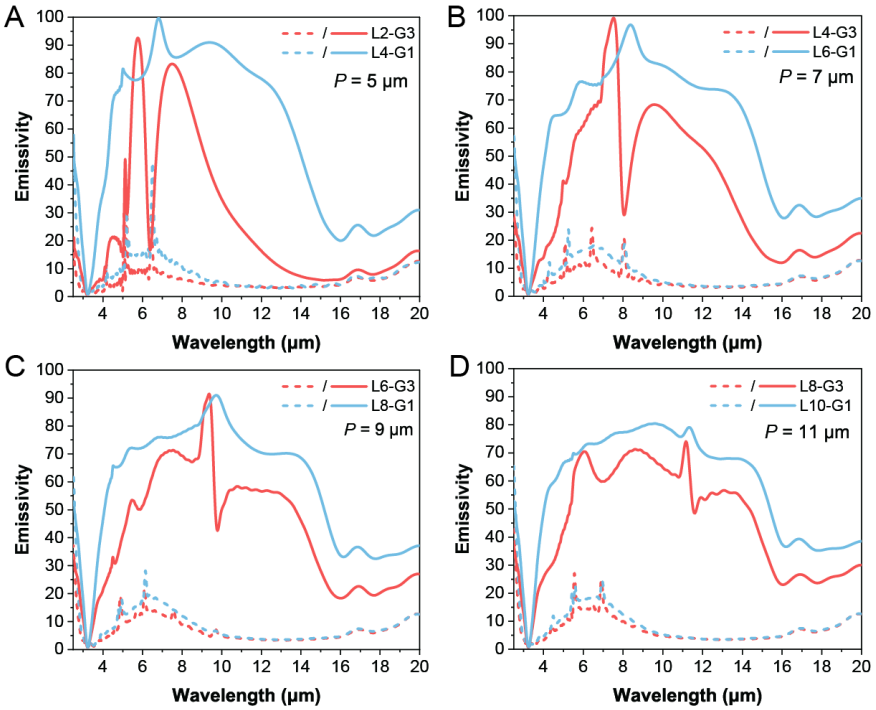

Fig. S5 A comparison for different *L* or *G* in the same period *P* (*P* = *L* + *G*), the dotted and solid lines represent the insulator and metal states of VO_2, respectively.

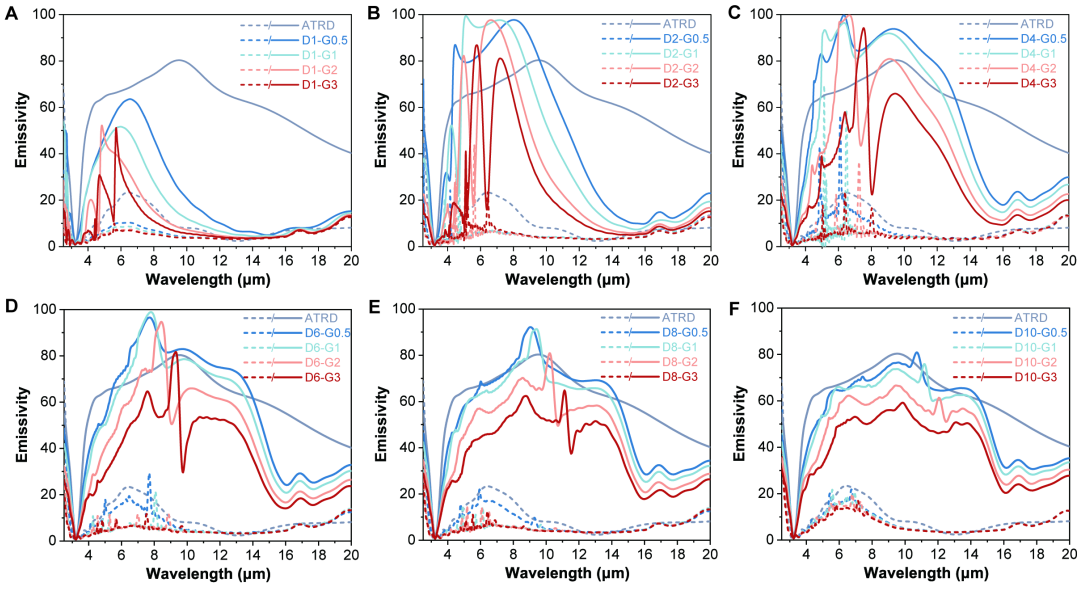

Fig. S6 The simulated emissivity spectrum ranges from 2.5 to 20 μm at different feature sizes *D* and *G* for ATMRD circular array structure (D*x*-G*y*). The dotted and solid lines represent the insulator and metallic states of VO_2, respectively.

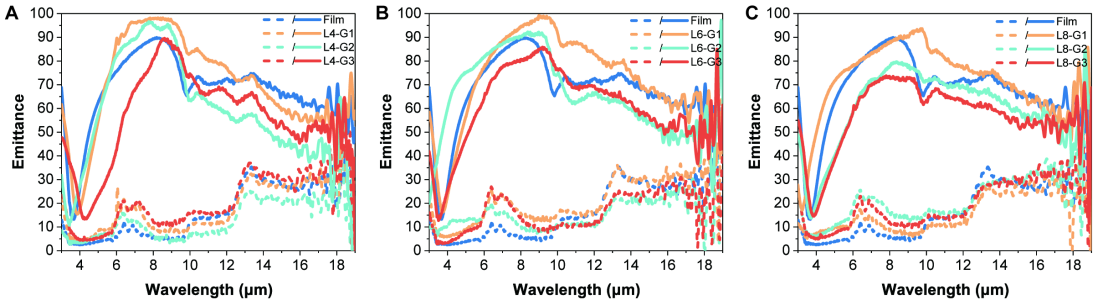

Fig. S7 The measured thermal emissivity spectral of ATMRD-L*x*-G*y* at 20℃ (dotted line) and 90℃ (solid line).

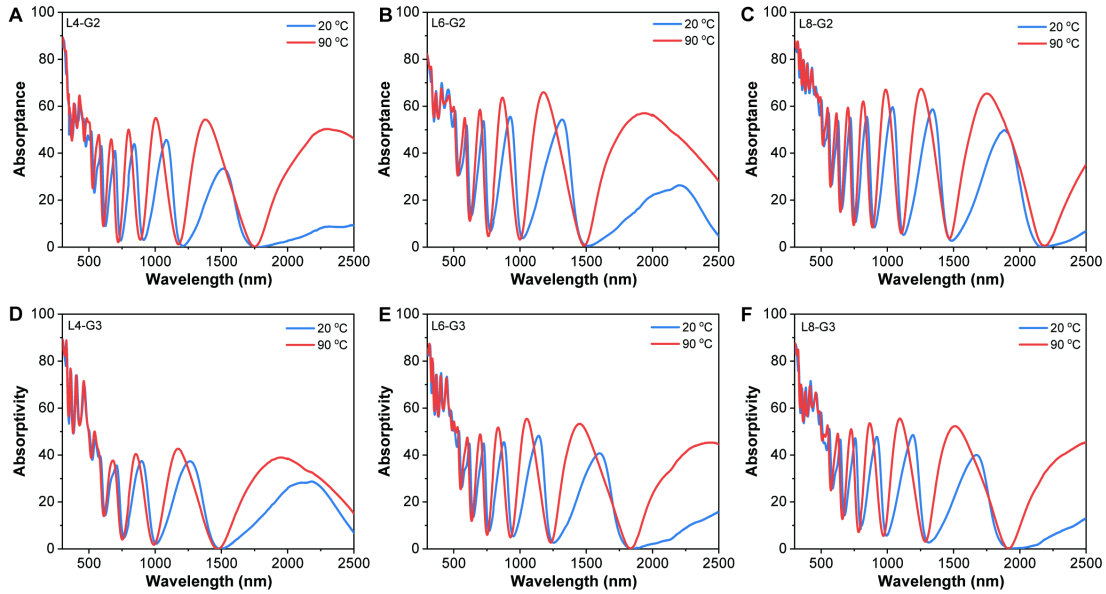

Fig. S8 The measured solar absorptance of ATMRD: (A) L4-G2, (B) L6-G2, (C) L8-G2, (D) L4-G3, (E) L6-G3, (F) L8-G3.

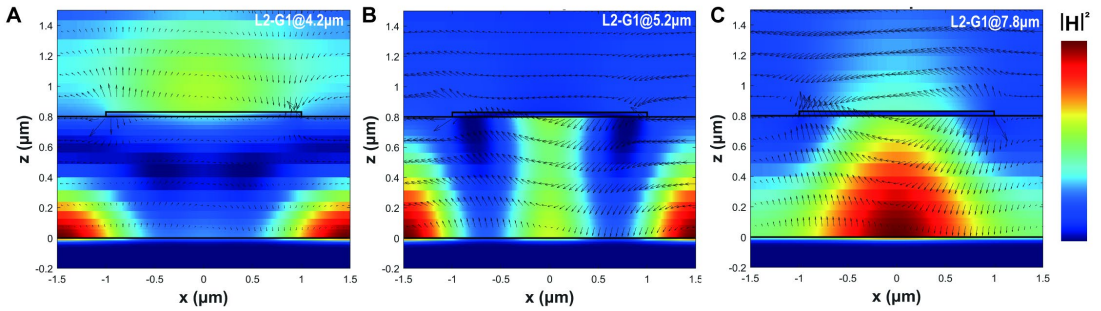

Fig. S9 Electromagnetic field distribution of the *x-z* cross-section of one array cell at different wavelengths for ATMRD L2-G1.

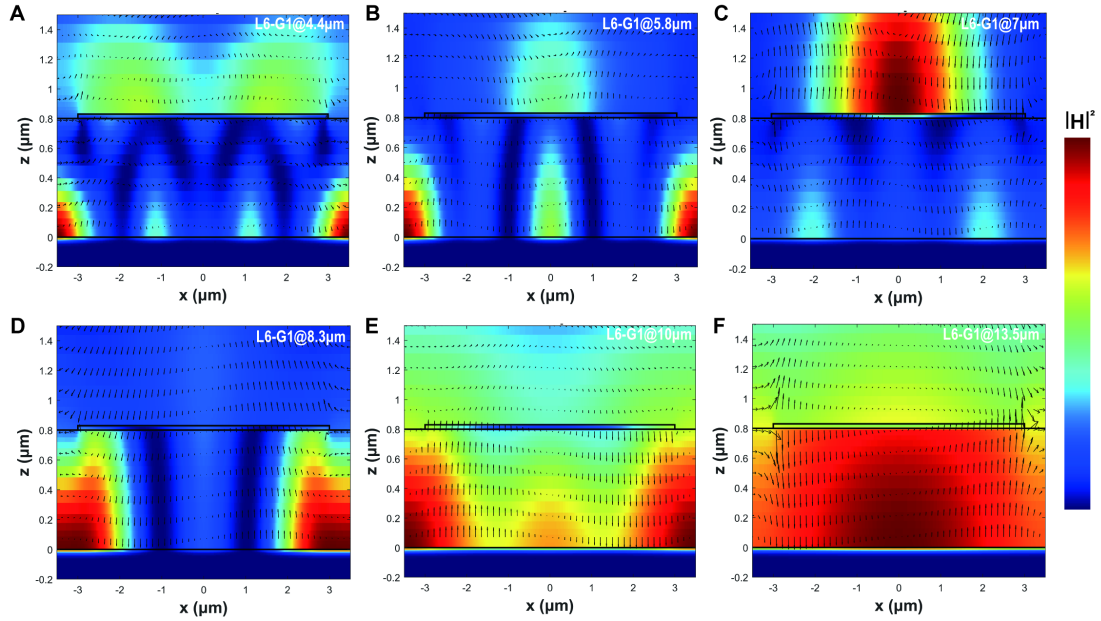

Fig. S10 Electromagnetic field distribution of the *x-z* cross-section of one array cell at different wavelengths for ATMRD L6-G1.

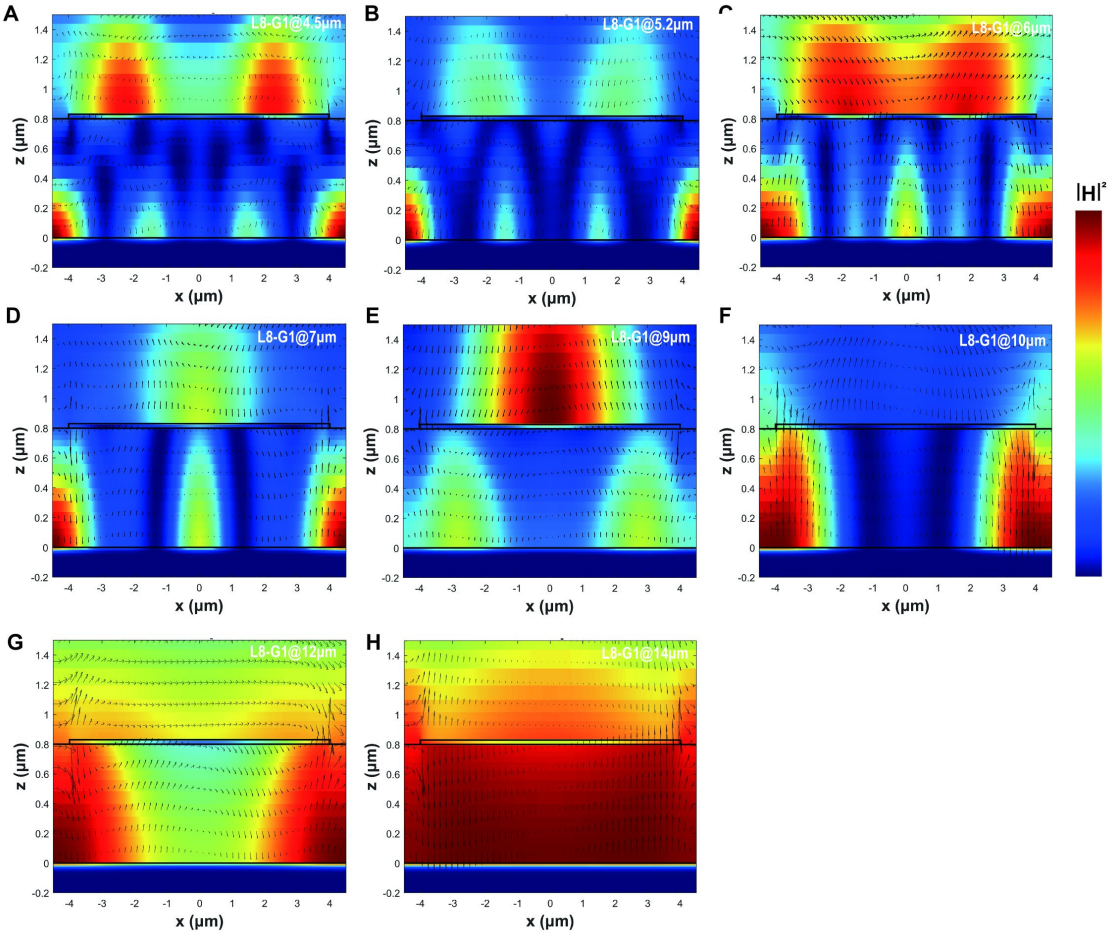

Fig. S11 Electromagnetic field distribution of the *x*-*z* cross-section of one array cell at different wavelengths for ATMRD L8-G1.

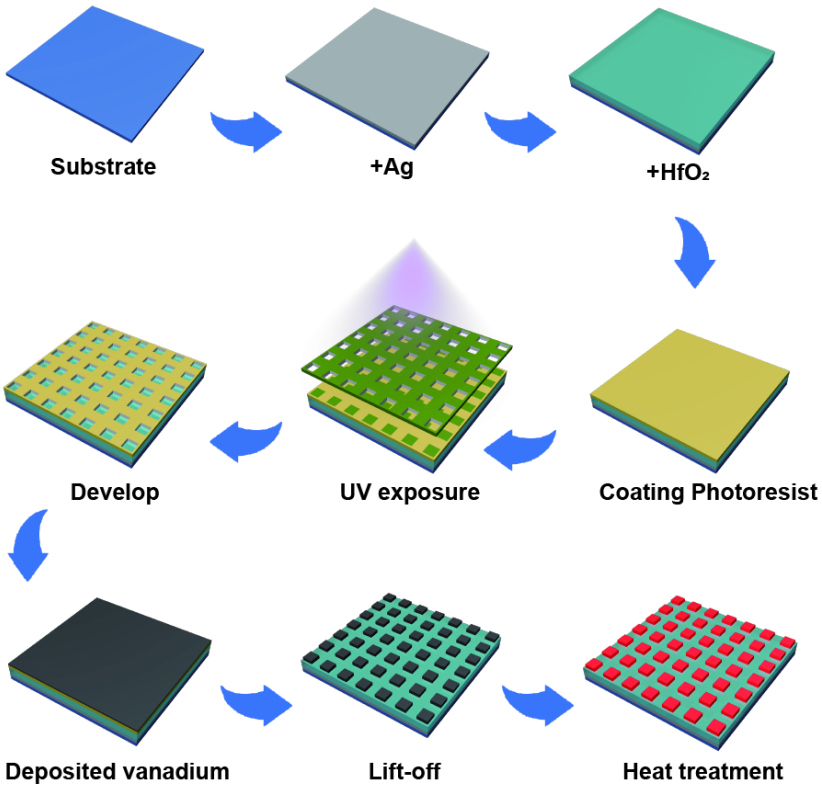

Fig. S12 The fabricated process of ATMRD by mask-filling engineering